Supporting Information for "Onset and withdrawal of the large-scale South Asian monsoon: A dynamical definition using change point detection"

Jennifer M. Walker,[1] Simona Bordoni[1]

Contents of this file

1. Text S1 to S2
2. Figures S1 to S9
3. Table S1

Introduction

This document provides further details on the domain selection, a summary of inter-annual variability of the CHP index, and additional supporting figures referenced in the main text.

---

[1]Environmental Science and Engineering,

California Institute of Technology,

Pasadena, California, USA.

Text S1: Domain Selection

To calculate the CHP index, we use the same domain (Fig. S1) as in our previous study [*Walker et al. 2015*], which we chose to represent the large-scale monsoon, including the precipitation maxima over India and the Bay of Bengal. We analyzed the sensitivity of our results to the domain choice and found that expanding or shrinking the latitude or longitude range did not substantially alter our findings, as long as we do not extend the domain past 100°E into Southeast Asia, where the monsoon variability is distinct from the SASM [*Walker et al. 2015*].

We chose 10–30°N as our latitude boundaries in order to include the latitudes in which the monsoonal circulation behaves coherently across most or all of the 60–100°E sector: hence, we exclude the topography to the north and the oceanic regions to the south whose seasonal variability is not consistent with the summer monsoon (less than half of annual rainfall occurring during June–September, Fig. S1). Although Kerala, a major regional component of the SASM, does extend south of 10°N, the surrounding oceanic regions—comprising the majority of the SASM sector south of 10°N—feature a different seasonal behavior (Fig. S1). This is confirmed when we re-calculate the CHP onset extending the domain to 5–30°N: the correlation with MOK actually decreases from 0.82 (Section 3.2 in the main text) to 0.76, indicating that 10°N is an appropriate southern boundary to represent the large-scale features we focus on here.

Text S2: Interannual Variability

Table S1 shows that monsoon season length is strongly correlated with both onset date (-0.76) and withdrawal date (0.80), indicating that longer monsoon seasons are associated

with earlier onset and later withdrawal, consistent with previous findings [*Goswami, 2005; Cook and Buckley, 2009*]. Early onset, late withdrawal, and longer season length are also correlated with increased cumulative rainfall over the monsoon season (Fig. S8, Table S1). This enhanced seasonal rainfall is approximately balanced by an increase in evaporation, leading to no significant correlations in the net precipitation (Fig. S8). The correlations in seasonal mean rates (Fig. S9, Table S1), while in some cases less robust, are all in the opposite direction as the correlations in the seasonal totals, indicating that season length—rather than changes in daily rates—is the primary cause for the observed correlations in Fig. S8. Thus, we conclude that the enhanced seasonal rainfall associated with early onsets, late withdrawals, and longer seasons is due to the increase in season length and is partially, but not completely, offset by a slight reduction in daily rainfall rates.

To investigate interannual variability in SASM timing associated with El Niño–Southern Oscillation (ENSO) variability, we use the Niño 3 index provided by the National Oceanic and Atmospheric Administration (NOAA) Climate Prediction Center (CPC) for the years 1980-2015. This index is a monthly average of sea surface temperatures from the Extended Reconstructed Sea Surface Temperature Version 4 [ERSST; *Huang et al., 2015*], averaged over the region 5°S–5°N, 150°W–90°W. We also conducted our analysis with the commonly used Niño 3.4 index (same as Niño 3 but averaged over 5°S–5°N, 170°W–120°W) and the results are all qualitatively similar but with weaker correlations, so we present the Niño 3 index, which displays the strongest correlations. We find that later onset dates are correlated with warm ENSO conditions in the previous March–May (MAM) and concurrent June–August (JJA), and shorter monsoon seasons are correlated with warm ENSO

conditions in JJA (Table S1), consistent with previous findings [*Fasullo and Webster, 2003; Goswami, 2005; Cook and Buckley, 2009; Noska and Misra, 2016*].

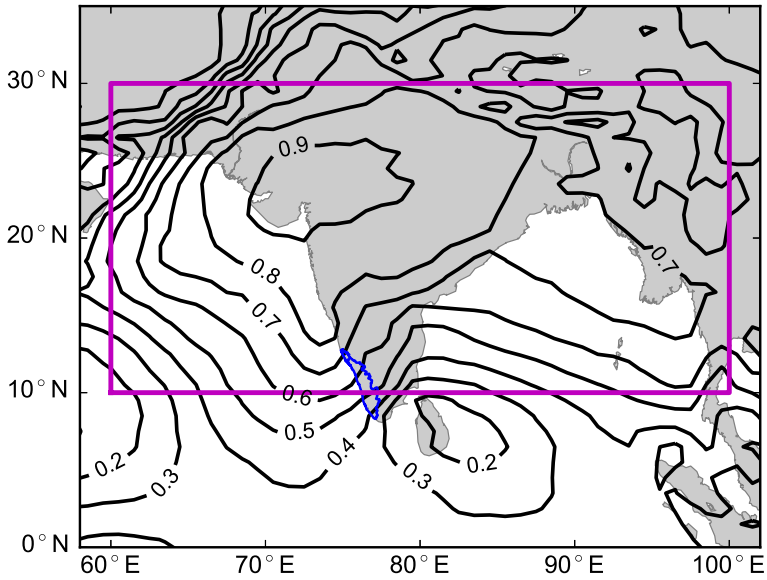

Figure S1. June–September (JJAS) fraction of yearly rainfall in GPCP climatology. The magenta rectangle shows the averaging region for the CHP index. Kerala state is outlined in blue.

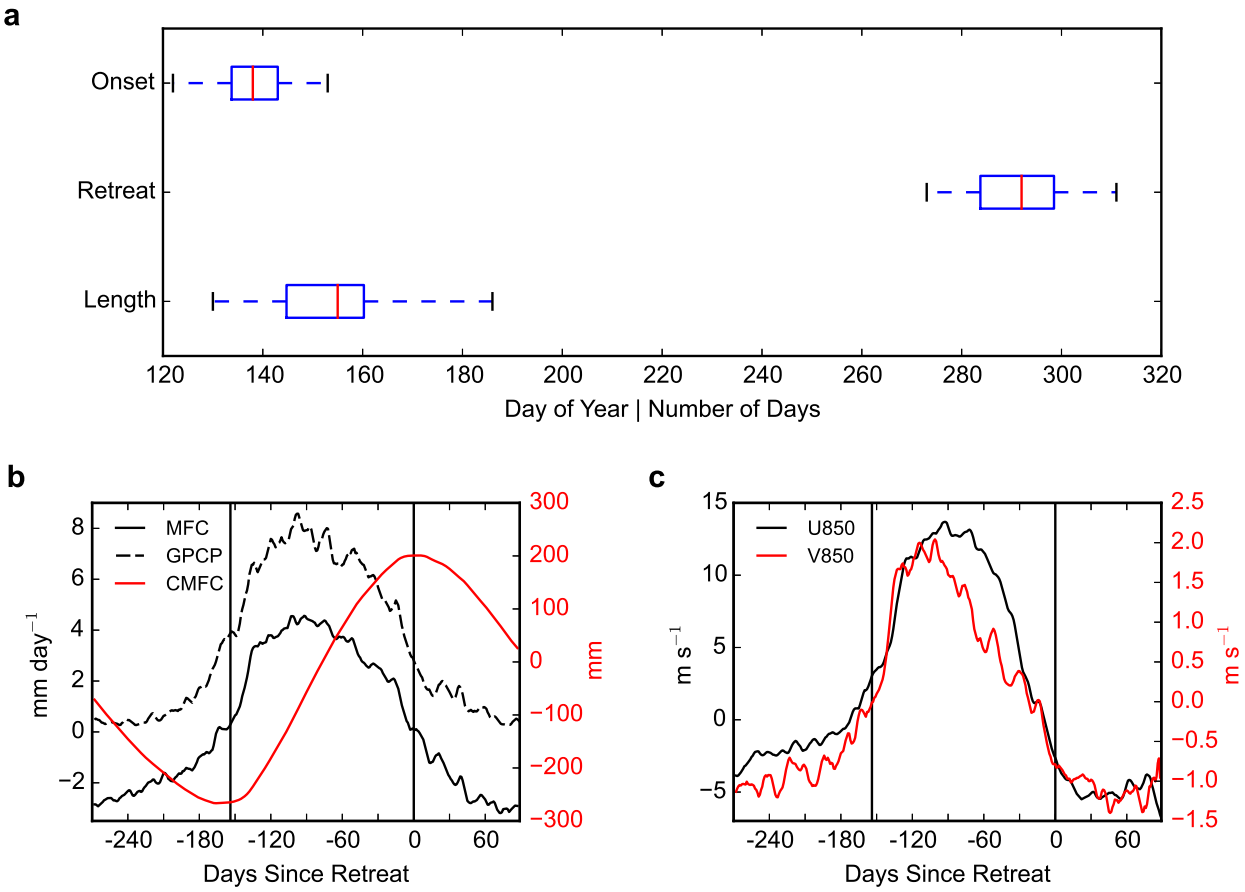

Figure S2. (a) Box-and-whisker plot for yearly onset dates, withdrawal dates, and season lengths defined by CHP. The blue boxes indicate the range between the 25th and 75th percentiles, with a red line for the median and whiskers indicating the total range. (b-c) Climatological composites of MERRA-2 and GPCP daily fields centered on withdrawal date, averaged 60-100°E, with vertical black lines indicating mean onset and withdrawal days. (b) Moisture budget averaged 10-30°N, showing MFC (solid black, mm day^{-1}), GPCP (dashed black, mm day^{-1}), and CMFC (red, mm). (c) 850 hPa zonal (black) and meridional (red) winds at 15°N (m s^{-1}).

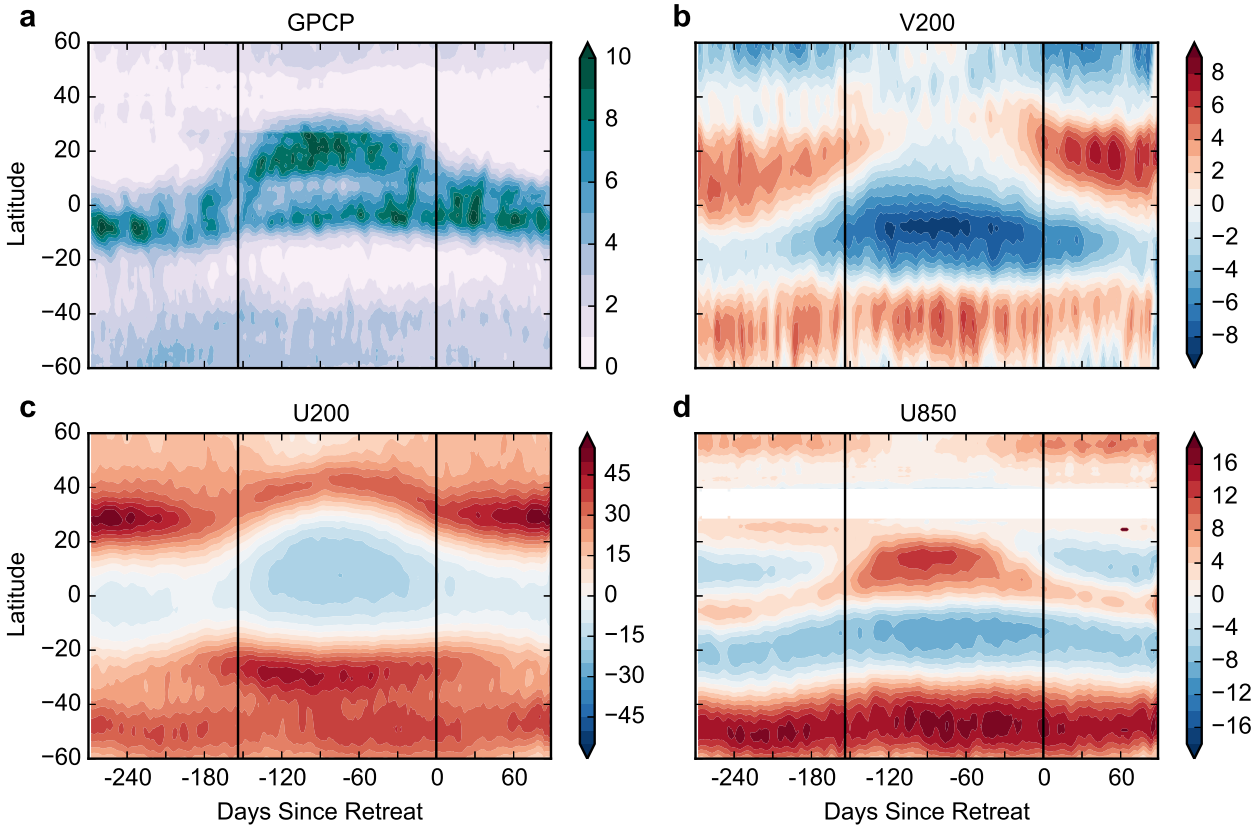

Figure S3. Seasonal evolution of (a) GPCP and (b-d) MERRA-2 climatological composites centered on withdrawal date, averaged 60-100°E: (a) precipitation (mm day^{-1}), (b) 200 hPa meridional wind (m s^{-1}), (c) 200 hPa zonal wind (m s^{-1}), and (d) 850 hPa zonal wind (m s^{-1}). Vertical black lines indicate mean onset and withdrawal days. Latitudes with less than 50% of grid points above the topography are masked out in (d).

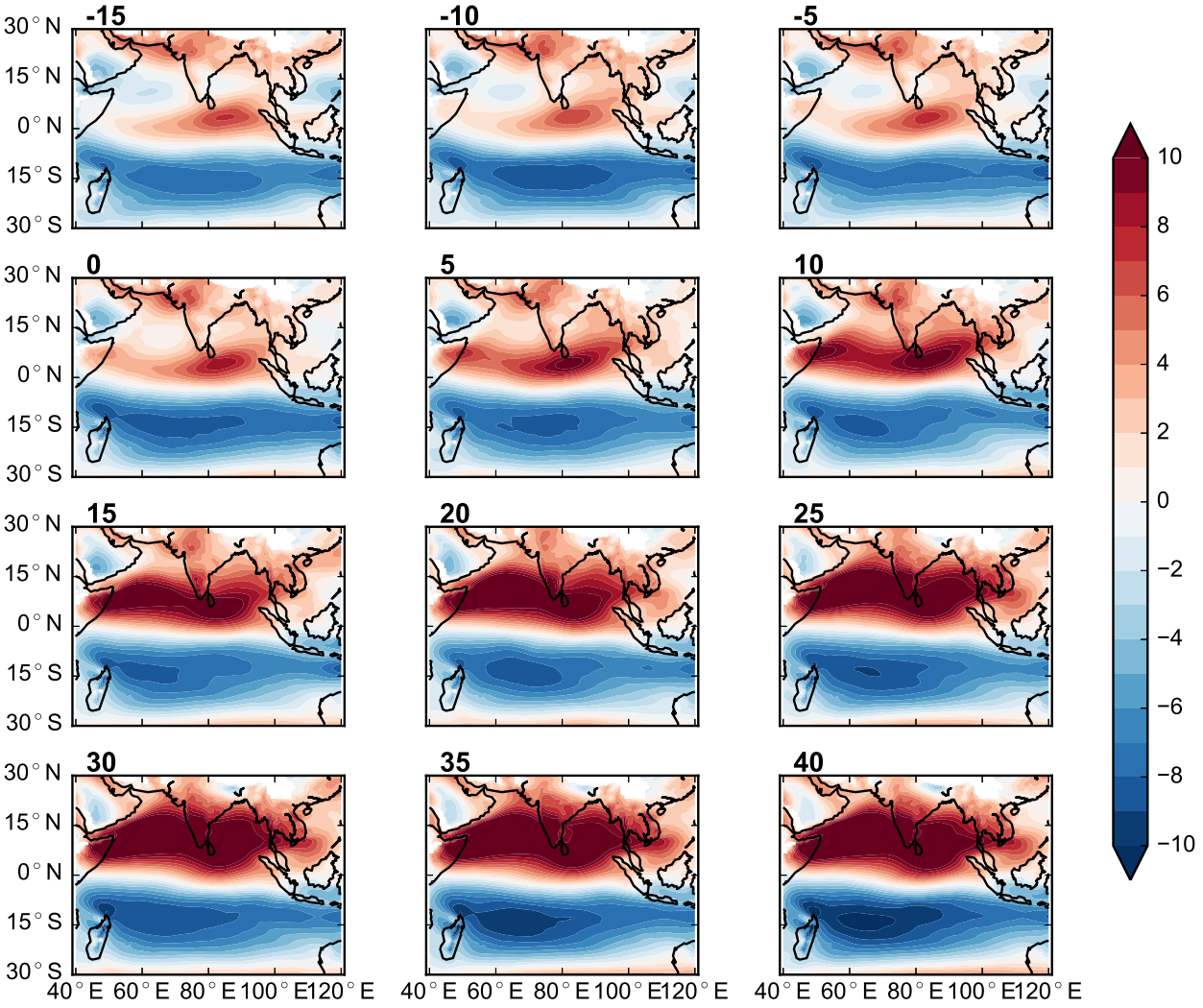

Figure S4. Maps of zonal wind (m s^{-1}) at 850 hPa in MERRA-2 climatological composites centered on onset date, for days -15 through 40.

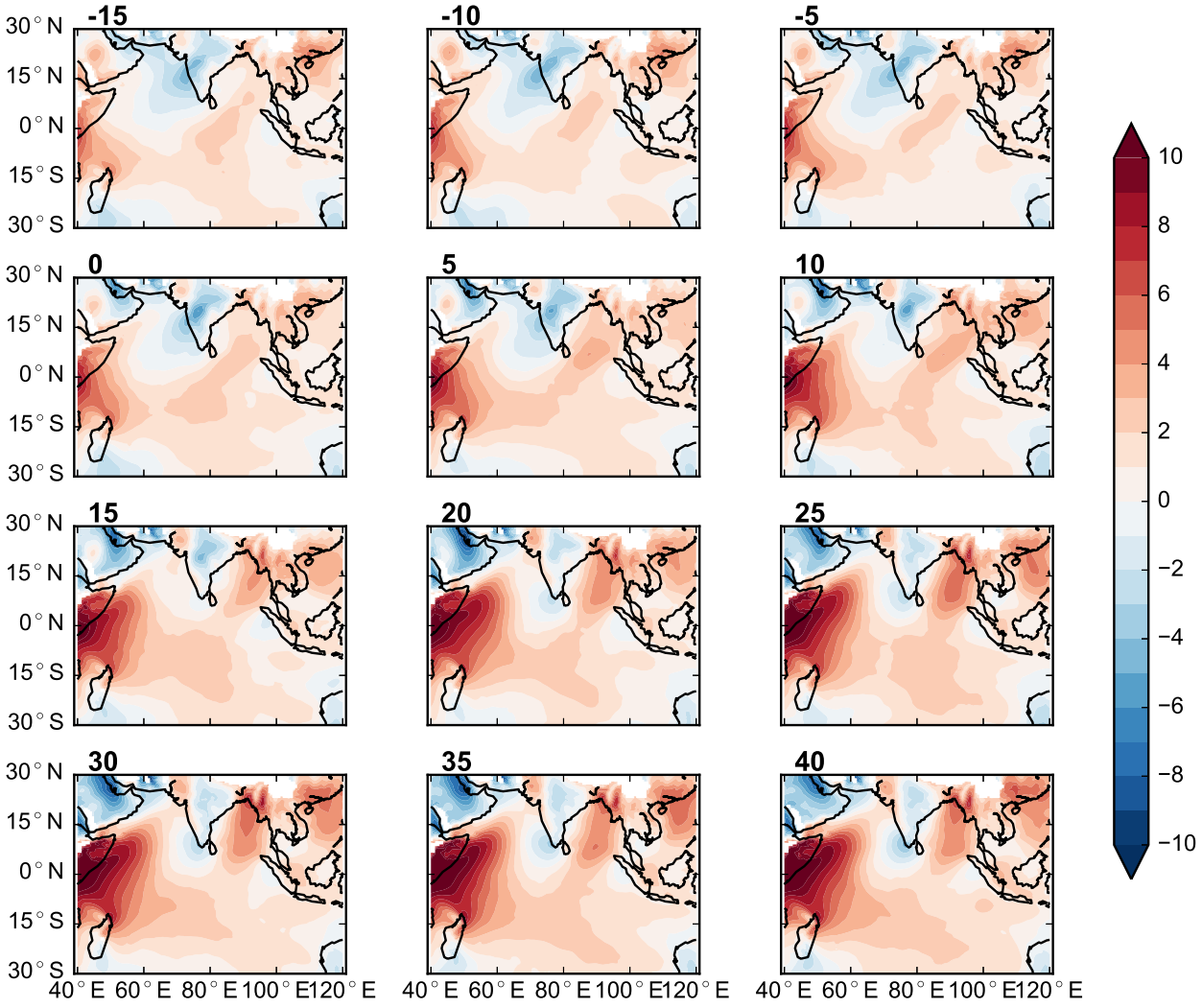

Figure S5. As in Fig. S4 but for meridional wind.

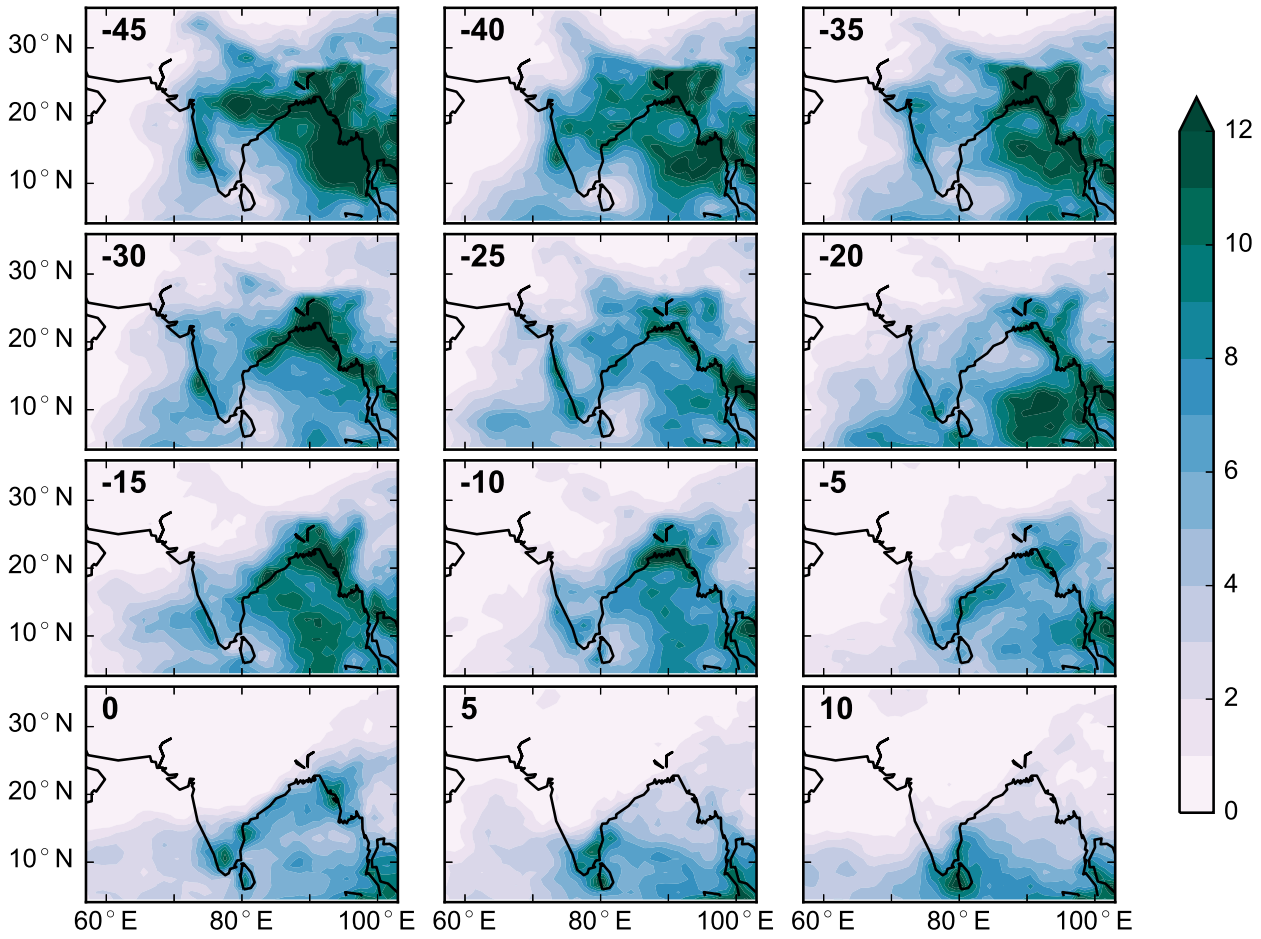

Figure S6. Maps of daily precipitation rates (mm day^{-1}) in GPCP climatological composites centered on withdrawal date, for days -45 through 10.

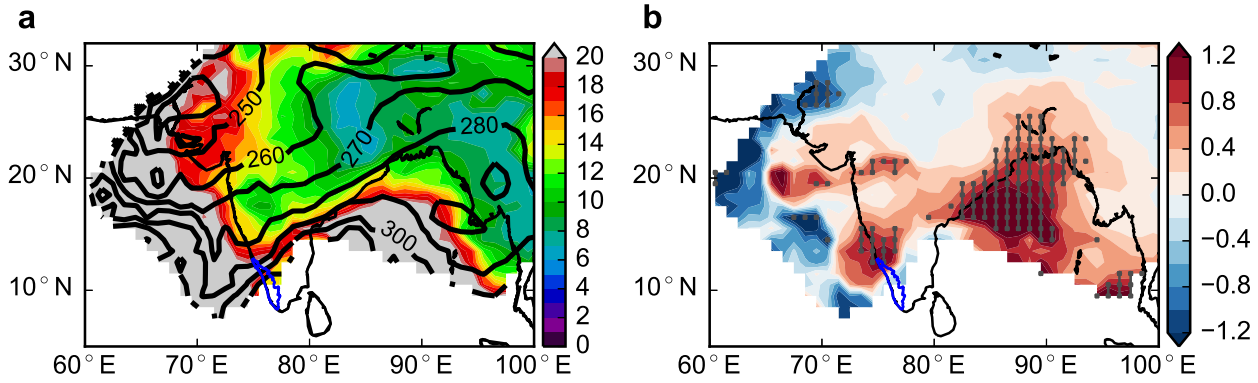

Figure S7. Local withdrawal dates defined with CHP method using GPCP precipitation. (a) Climatological mean (contours) and standard deviation (colors) of onset dates. (b) Regression coefficients (day day^{-1}) of local withdrawal dates onto large-scale CHP withdrawal index, with gray stippling indicating the regions where the correlation is significant at the 5% level. Kerala state is outlined in blue.

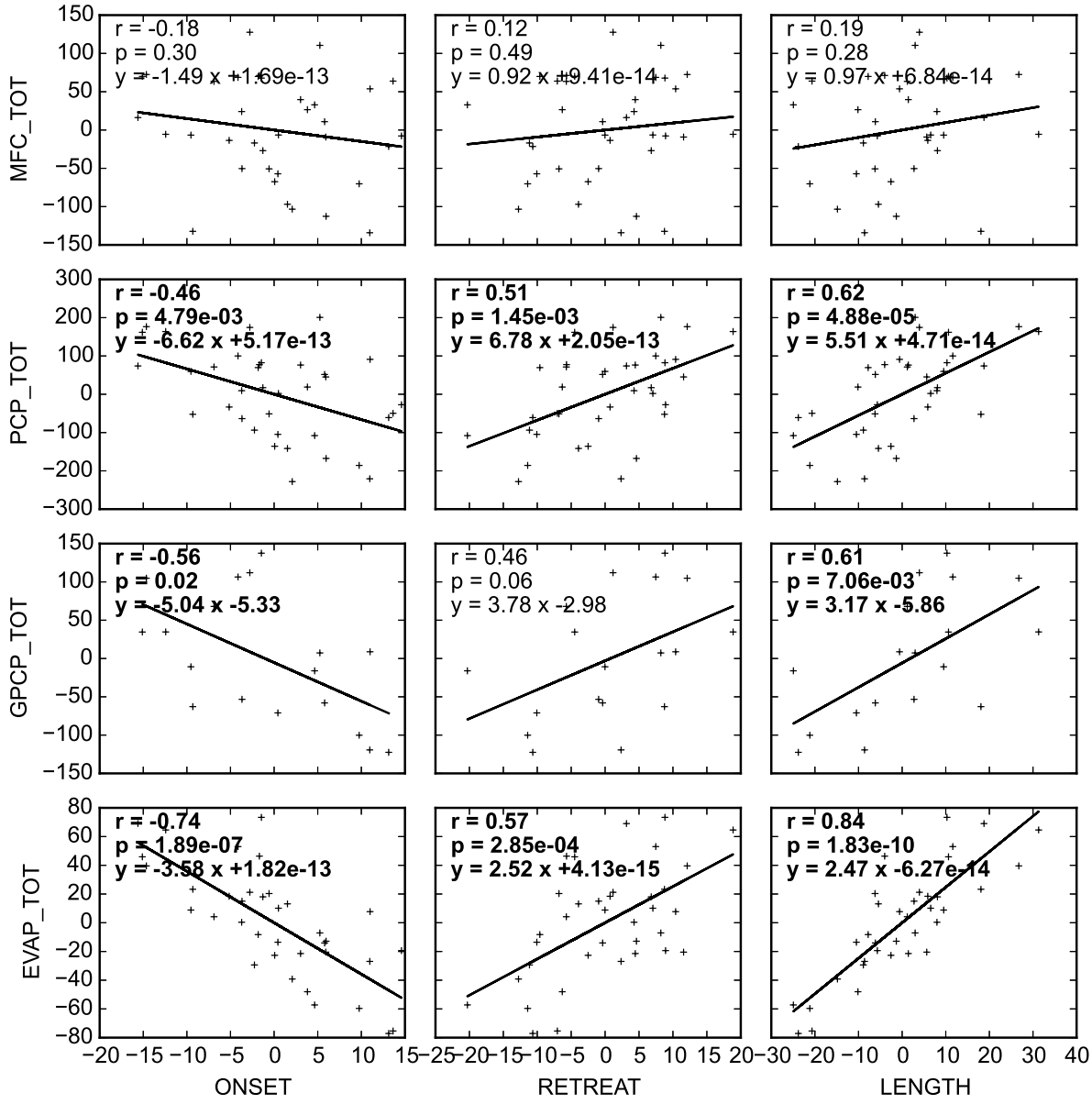

Figure S8. Scatter plots and linear regressions of detrended monsoon season totals (mm), from onset to retreat in each year, of MERRA-2 moisture flux convergence (MFC_TOT), MERRA-2 precipitation (PCP_TOT), GPCP precipitation (GPCP_TOT), and MERRA-2 evaporation (EVAP_TOT), averaged 10–30°N, 60–100°E vs. detrended SASM onset, retreat, and season length (days). Note that the GPCP dataset is shorter than MERRA-2, so higher correlation coefficients are required for statistical significance at the 5% level.

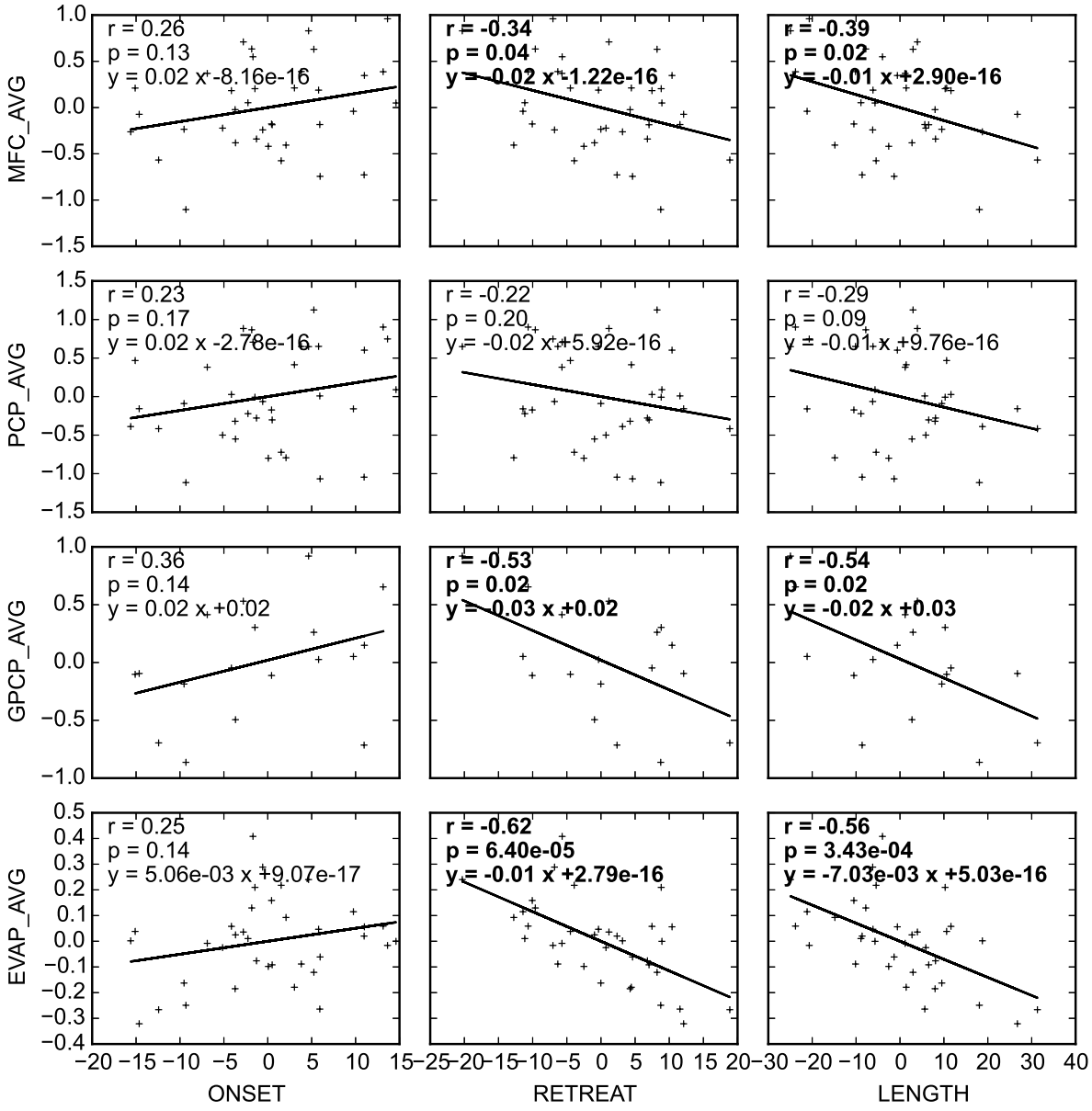

Figure S9. Scatter plots and linear regressions of detrended seasonal mean rates (mm day^{-1}), averaged from onset to retreat in each year, of MERRA-2 moisture flux convergence (MFC_AVG), MERRA-2 precipitation (PCP_AVG), GPCP precipitation (GPCP_AVG), and MERRA-2 evaporation (EVAP_AVG), averaged 10–30°N, 60–100°E vs. detrended SASM onset, retreat, and season length. Note that the GPCP dataset is shorter than MERRA-2, so higher correlation coefficients are required for statistical significance at the 5% level.

Table S1. Interannual correlation coefficients between CHP indices, GPCP seasonal total and mean rainfall (from onset to withdrawal each year, averaged 10–30°N, 60–100°E), and ENSO indices. Values significant at the 5% level are indicated in bold. Note that the GPCP dataset is shorter than the other indices, so higher correlation coefficients are required for statistical significance at the 5% level.

	Onset Date	Withdrawal Date	Season Length
Onset Date	**1.00**	-0.22	**-0.76**
Withdrawal Date	-0.22	**1.00**	**0.80**
Season Length	**-0.76**	**0.80**	**1.00**
GPCP Seasonal Total Rainfall	**-0.56**	0.46	**0.61**
GPCP Seasonal Mean Rainfall	0.36	**-0.53**	**-0.54**
NINO3 MAM	**0.41**	0.08	-0.20
NINO3 JJA	**0.39**	-0.24	**-0.40**